


Quasiloclization dynamics in a Fibonacci quantum rotor

Sourav Bhattacharjee ^{*}, Souvik Bandyopadhyay , and Amit Dutta

Department of Physics, Indian Institute of Technology Kanpur, Kanpur 208016, India

 (Received 22 November 2021; revised 25 April 2022; accepted 22 July 2022; published 8 August 2022)

We analyze the dynamics of a quantum kicked rotor (QKR) driven with a binary Fibonacci sequence of two distinct drive amplitudes. While the dynamics at low drive frequencies is found to be diffusive, a long-lived preergodic regime emerges in the other limit. Furthermore, the dynamics in this preergodic regime can be associated with the onset of a dynamical quasiloclization, similar to the dynamical localization observed in a regular QKR. We establish that this peculiar behavior arises due to the presence of localized eigenstates of an approximately conserved effective Hamiltonian, which drives the evolution at Fibonacci instants. However, the effective Hamiltonian picture does not persist indefinitely, and the dynamics eventually becomes ergodic after asymptotically long times.

DOI: [10.1103/PhysRevA.106.022206](https://doi.org/10.1103/PhysRevA.106.022206)

I. INTRODUCTION

The quantum kicked rotor (QKR) [1,2] is central to understanding the basics of quantum chaos and has been subjected to a plethora of analytical [3–8] as well as experimental [9–15] investigations over the years [16–19]. In contrast to the classical rotor, which shows a transition from a regular phase to the chaotic phases, the QKR seemingly exhibits a nonergodic behavior. Using Floquet theory [20–23], it is found that the eigenstates of the effective Floquet Hamiltonian are exponentially localized in the angular momentum space. This, together with quantum interference effects, leads to dynamical localization in periodic QKRs. Remarkably, the nonergodicity in the dynamics is manifested for any finite amplitude and frequency of the kicks (see Appendix A for a brief recapitulation).

The *dynamical localization* observed in the QKR has far-reaching implications. It was realized that this localization can be exactly mapped to the spatial Anderson localization problem [24] in one dimension [4,5]. However, the Anderson problem in more than one dimension is known to exhibit a localization-delocalization transition [25]. In the case of the QKR, similar transitions were also found, albeit in a slightly modified version in which the rotor is driven with three incommensurate frequencies. In this case, the rotor Hamiltonian with time-dependent kick amplitude is first mapped to a three-dimensional rotor [26] with time-independent kick amplitudes at equal time intervals [27]. The temporal evolution at stroboscopic intervals is then found to be governed by a Floquet Hamiltonian, having exponentially localized eigenstates in the localized phase. Thus it came to be accepted that the localization-delocalization transition in a more-than-one-dimensional Anderson problem can manifest in the rotor dynamics if the “temporal” dimension is increased, i.e., when driven with multiple incommensurate frequencies.

In this paper, we show that a quasiloclization-to-delocalization transition can also manifest in the QKR driven with a single frequency but where the kick amplitudes at subsequent stroboscopic instants follow a binary Fibonacci sequence. We dub this variant of the QKR the *Fibonacci quantum kicked rotor* (FQKR). As our main result, we show the emergence of a “preergodic” regime in the limit of high drive frequencies during which the wave function of the FQKR remains “dynamically quasiloclized” in the angular momentum space. Although the dynamics eventually becomes ergodic, the preergodic regime has a long experimentally relevant lifetime, which further increases with the kicking frequency. However, at lower drive frequencies, the dynamics is always found to be ergodic. We note that the Fibonacci drive [28,29] has been extensively used to explore the consequences of temporal quasiperiodicity in various out-of-equilibrium systems [30–40].

An important distinction in the approach of our work from previously studied rotors driven at incommensurate frequencies [27,41] is that the quasiperiodicity in our model is externally enforced through a binary sequence of kick amplitudes. This is manifestly different from previous works where, for example, quasiperiodicity is indirectly enforced through quasiperiodic phase shifts of the position operator, keeping the kick amplitude constant [27]. Secondly, the quasiloclization observed in the preergodic regime is not discernible from a standard Floquet analysis of the evolution operator. Rather, it follows from the existence of *self-similar eigenstates* and is thus different from hitherto observed dynamical localization in the conventional QKR. Crucially, we note that the existence of a preergodic regime is unique to the FQKR. Furthermore, we have verified that the quasiloclization is not found for aperiodic binary sequences (see Appendix B for details).

The rest of this paper is organized as follows: The FQKR model is introduced in Sec. II. In Sec. III, we present results from the numerical simulation of the dynamics of the FQKR. The quasiloclization behavior observed is explained through a perturbative analysis of the time-evolution operator

^{*}sourav.offc@gmail.com

in Sec. IV. Finally, we summarize our results in Sec. V. In addition, Appendixes A–E recapitulate known results, especially those of the regular QKR, and also outline the detailed calculations needed to arrive at some of the results presented in this paper.

II. MODEL

The QKR is represented by the Hamiltonian

$$H(t) = \frac{\hat{l}^2}{2I} + \cos \hat{\theta} \sum_{N=0}^{\infty} K_N \delta(t - NT), \quad (1)$$

where $\hat{\theta}$ and \hat{l} are the angular displacement and angular momentum operators, respectively, while I is the moment of inertia of the rotor. The rotor evolves freely with time period T between subsequent kicks of strength K_N , which act on the rotor at the stroboscopic instants NT , where $N \in \mathbb{Z}^+$. However, in our case, we consider $K_N \in \{\mathcal{K}_1, \mathcal{K}_2\}$, and thus $\{K_N\}_{N=1}^{\infty} \equiv K_1, K_2, \dots$ constitutes a binary sequence.

If the rotor is initially in a state $|\psi(t=0)\rangle = |\psi_0\rangle$, the state of the system at the N th stroboscopic instant (just before the N th kick) is thus given by

$$|\psi_N\rangle \equiv |\psi(NT)\rangle = U(NT, 0) |\psi_0\rangle = U_N U_{N-1} \cdots U_1 |\psi_0\rangle, \quad (2)$$

U_N being the the unitary operator propagating the system from the $(N-1)$ th to the N th time interval given by

$$U_N = \mathcal{T} \exp\left(-i \int_{(N-1)T}^{NT} H(t) dt\right) = e^{-i \frac{\hat{l}^2}{2} \tau} e^{-i K_N \cos \hat{\theta}}, \quad (3)$$

where \mathcal{T} is the time-ordering operator. Note that we have set $\hbar = 1$ and rescaled the time period T to a dimensionless parameter $\tau = T/I$ [42]. In the conventional QKR, $K_N = \mathcal{K}$ for all N ; the dynamics is then equivalent to an evolution under the Floquet propagator $U_F = e^{-i \frac{\hat{l}^2}{2} \tau} e^{-i \mathcal{K} \cos \hat{\theta}} = e^{-i H_F \tau}$, such that Eq. (2) can be written as $|\psi_N\rangle = e^{-i H_F N} |\psi_0\rangle$. For a finite \mathcal{K} , the eigenstates of the Floquet Hamiltonian H_F are exponentially localized in the angular momentum space. This leads to a localization of the wave function in the angular momentum space, and the dynamics is consequently nonergodic (see Appendix A for details).

Referring to Eq. (1), let us now introduce the FQKR as a quantum rotor where the sequence of kicks driving the rotor follows the Fibonacci sequence

$$K_N = \mathcal{K}_1 + (2 - \gamma(N)) \frac{\Delta \mathcal{K}}{2}, \quad (4)$$

where $\Delta \mathcal{K} = \mathcal{K}_2 - \mathcal{K}_1$. The generating function is given by $\gamma(N) = \lfloor (N+1)G \rfloor - \lfloor NG \rfloor$, where $\lfloor x \rfloor$ denotes the greatest integer less than or equal to x and G is the golden mean $G = (\sqrt{5} + 1)/2$. $\gamma(N)$ can thus assume a value of 0 or 2. To see that Eq. (4) generates a Fibonacci sequence, let us look at the sequences generated at the *Fibonacci instants* $\mathcal{N} \in \mathbb{Z}^+$. The stroboscopic instant corresponding to the \mathcal{N} th Fibonacci instant is given by the function $F(\mathcal{N})$ which satisfies $F(\mathcal{N}) = F(\mathcal{N}-1) + F(\mathcal{N}-2)$. Thus we have $F(1) = 1$, $F(2) = 2$, $F(3) = 3$, $F(4) = 5$, $F(5) = 8$, $F(6) = 13$, and so on. As-

suming that $K_1 = \mathcal{K}_1$, we therefore find

$$\begin{aligned} \{K_N\}_{N=1}^{F(1)} &\equiv S_1 = \mathcal{K}_1, \\ \{K_N\}_{N=1}^{F(2)} &\equiv S_2 = \mathcal{K}_1 \mathcal{K}_2, \\ \{K_N\}_{N=1}^{F(3)} &\equiv S_3 = \mathcal{K}_1 \mathcal{K}_2 \mathcal{K}_1, \\ \{K_N\}_{N=1}^{F(4)} &\equiv S_4 = \mathcal{K}_1 \mathcal{K}_2 \mathcal{K}_1 \mathcal{K}_1 \mathcal{K}_2, \\ \{K_N\}_{N=1}^{F(5)} &\equiv S_5 = \mathcal{K}_1 \mathcal{K}_2 \mathcal{K}_1 \mathcal{K}_1 \mathcal{K}_2 \mathcal{K}_1 \mathcal{K}_2 \mathcal{K}_1, \end{aligned} \quad (5)$$

where S_n denotes the n th Fibonacci sequence, satisfying $S_n = S_{n-1} S_{n-2}$.

III. NUMERICAL RESULTS

For numerical simulations, the initial state is chosen to be a normalized Gaussian quantum state centered around the angular momentum l_0 , $\psi_0(l) = (\frac{2}{\pi})^{\frac{1}{4}} e^{-(l-l_0)^2}$, unless otherwise stated. Furthermore, we employ a truncated basis of angular momentum states for the numerics so that $(l_0 - R/2) \leq l \leq (l_0 + R/2 - 1)$, where R is chosen to be large enough to ensure normalization of the wave function at all times. For dynamical localized wave functions, this is ensured by choosing $R \gg \xi$, where ξ is the localization length. The temporal evolution of the kinetic energy $\langle l^2 \rangle$ for the FQKR with $l_0 = 0$ is shown in Fig. 1(a). We find that the kinetic energy grows diffusively at low frequencies (high τ) and localizes at high, but finite frequency $\tau \leq 0.01$. However, as shown in Fig. 1(b), the localization does not persist indefinitely, and a diffusive behavior emerges eventually. Nevertheless, the time after which this happens rapidly increases as the drive frequency increases. We have numerically verified that the results remain qualitatively the same for different choices of \mathcal{K}_1 and \mathcal{K}_2 . Furthermore, as shown in Appendix C, the above results remain qualitatively the same for different choices of l_0 .

IV. PERTURBATIVE ANALYSIS

The quasilocalized behavior observed in the limit of high frequencies suggests that there might possibly exist an effective Hamiltonian, similar to the Floquet Hamiltonian, which governs the dynamics of the FQKR in this limit. Importantly, the eigenstates of this effective Hamiltonian should also be exponentially localized in the angular momentum space. To verify whether this is indeed the case, we resort to a perturbative analysis of the unitary evolution operator, with τ as the small parameter.

A. Perturbative expansion of the unitary operator

For $\tau \ll 1$, the unitary operator U_N driving the evolution between the $(N-1)$ th and N th kicks can be written as $U_N = e^{-i \frac{\hat{l}^2}{2} \tau} e^{-i K_N \cos \hat{\theta}} \approx e^{-i L_{1,2}}$, where $L_{1,2}$ is calculated from a Baker-Campbell-Hausdorff (BCH) expansion of U_N ,

$$\begin{aligned} L_{1,2} &= \mathcal{K}_{1,2} \cos \hat{\theta} + \frac{\tau}{2} \left[\hat{l}^2 + \frac{\mathcal{K}_{1,2}}{2} (\hat{l} \sin(\hat{\theta}) + \sin(\hat{\theta}) \hat{l}) \right. \\ &\quad \left. + \frac{\mathcal{K}_{1,2}^2}{12} \sin^2(\hat{\theta}) \right] + O(\tau^2), \end{aligned} \quad (6)$$

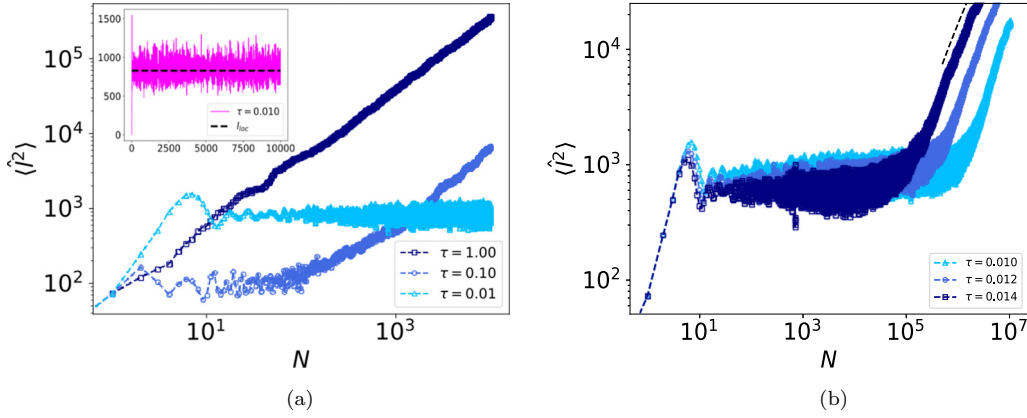


FIG. 1. (a) The kinetic energy of a FQKR grows diffusively at lower drive frequencies and dynamically quasilocates at high frequency ($\tau < 0.1$). The inset shows that the fluctuations in the quasilocated (preergodic) regime are evenly spread about the mean kinetic energy calculated from the perturbation analysis (black dashed line) using Eq. (8). (b) The quasilocalization is destroyed, and an ergodic behavior is found to emerge at very long times. This can be seen from the linear growth of the kinetic energy with unit slope for $N > 10^5$. The black dashed line with unit slope is provided for visual reference. Furthermore, the time after which localization is destroyed progressively increases as the frequency (τ^{-1}) is increased. The kick amplitudes chosen for the plot are $\mathcal{K}_1 = 10$, $\mathcal{K}_2 = 12$, and the initial state is chosen to be the angular momentum eigenstate $|\psi_0\rangle = |l = 0\rangle$.

having retained terms only up to linear order in τ . It can be shown (see Appendix D) that the propagator driving the evolution up to the N th stroboscopic instant assumes the form $U(N, 0) = e^{-iH_N N}$, where the Hamiltonian H_N takes the form

$$H_N = \frac{\alpha(N)}{N}L_1 + \frac{\beta(N)}{N}L_2 + \frac{\delta(N)}{N}[L_2, L_1] + \frac{\eta_1(N)}{N}[L_1, [L_1, L_2]] + \frac{\eta_2(N)}{N}[L_2, [L_2, L_1]] + O(\tau^2). \tag{7}$$

The coefficients $\alpha(N)/N$, $\beta(N)/N$, $\delta(N)/N$, $\eta_1(N)/N$, and $\eta_2(N)/N$, henceforth referred to as the *normalized expansion coefficients* (NECs), depend on the exact form of the binary sequence. The NECs for the Fibonacci sequence are evaluated in detail in Appendix D.

From Fig. 2(a), we see that while $\beta(N)/N$ [also $\alpha(N)/N = 1 - \beta(N)/N$, as shown in Appendix D] saturates to a constant value, $\delta(N)/N$ exhibits small amplitude fluctuations about a mean value. On the other hand, the growth of the coefficients $\eta_1(N)/N$ and $\eta_2(N)/N$ with N is unbounded. The Hamiltonian

H_N , as defined in Eq. (7), is therefore N dependent and is not a conserved quantity, unlike the Floquet Hamiltonian. However, a different picture emerges if we observe the behavior of the NECs at Fibonacci instants \mathcal{N} . In this case, as shown in Fig. 2(b), the coefficients $\beta(F(\mathcal{N}))/F(\mathcal{N})$, $\alpha(F(\mathcal{N}))/F(\mathcal{N})$, and $\delta(F(\mathcal{N}))/F(\mathcal{N})$ are found to saturate to steady values for $\mathcal{N} > 10$ while the coefficients $\eta_1(F(\mathcal{N}))/F(\mathcal{N})$ and $\eta_2(F(\mathcal{N}))/F(\mathcal{N})$ oscillate between a pair of constant values. Thus, for $\mathcal{N} > 10$, one can substitute $H_{N=F(\mathcal{N})} = H_{\text{Fi}}$ (see Appendix E for details), where H_{Fi} is an *effective Fibonacci Hamiltonian* which governs the dynamics of the rotor at Fibonacci instants. Furthermore, as shown in Fig. 3, the eigenstates of H_{Fi} are also localized in the angular momentum basis. It therefore follows that the dynamics of FQKR should mimic that of the regular QKR when observed at Fibonacci instants $N = F(\mathcal{N})$ and when terms of order $O(\tau^2)$ can be neglected in the perturbative analysis. Nevertheless, the existence of an effective Fibonacci Hamiltonian at Fibonacci instants does not guarantee the persistent localization seen throughout the evolution. In fact, the localization in between two subsequent Fibonacci instants is particularly surprising, given that

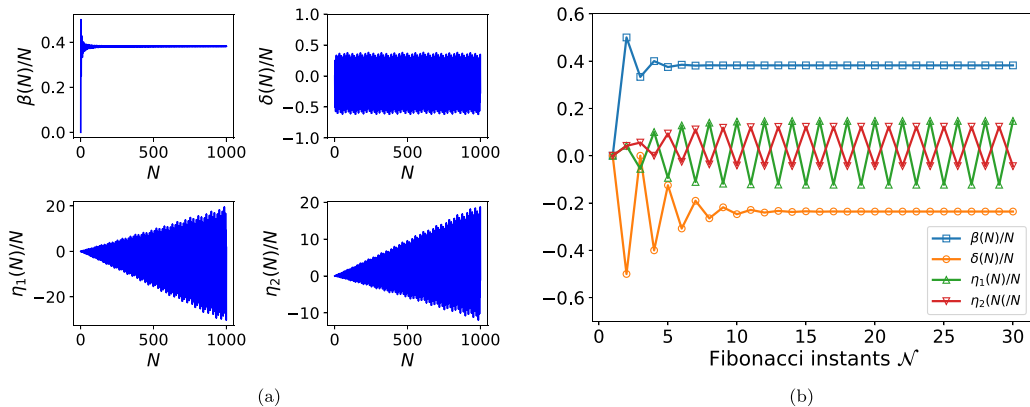


FIG. 2. The normalized expansion coefficients defined in Eq. (7) at (a) stroboscopic instants N and (b) Fibonacci instants \mathcal{N} .

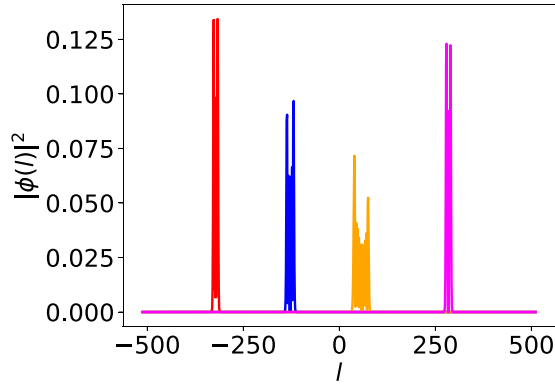


FIG. 3. Typical eigenstates of the effective Fibonacci Hamiltonian H_{Fi} , peaked around different values of l , for $\mathcal{K}_1 = 10$, $\mathcal{K}_2 = 12$, and $\tau = 0.01$. The eigenstates are found to be localized in the angular momentum space.

the growth of the coefficients $\eta_1(N)/N$ and $\eta_2(N)/N$ is unbounded when observed at stroboscopic instants, as already seen in Fig. 2(a).

This apparent contradiction can be explained if one inspects the self-similar or fractal nature of the Fibonacci sequence. To elaborate, let us consider the evolution between two subsequent Fibonacci instants \mathcal{N}^* and $\mathcal{N}^* + 1$, where we assume $F(\mathcal{N}^*) \gg 1$ so as to ensure that the NECs have saturated to their mean values. From Eq. (5), we note that the sequence of kicks up to $N^* = F(\mathcal{N}^*)$ and $N^{**} = F(\mathcal{N}^* + 1)$ is given by $S_{\mathcal{N}^*}$ and $S_{\mathcal{N}^*+1}$, respectively. However, by construction, $S_{\mathcal{N}^*+1} = S_{\mathcal{N}^*} S_{\mathcal{N}^*-1}$, which immediately implies that the sequence of kicks between N^* and N^{**} is nothing but the sequence $S_{\mathcal{N}^*-1}$.

The dynamics of the rotor in between two Fibonacci instants can now be analyzed as follows. Given a localized wave function $|\psi_{N^*}\rangle$, the evolution of this wave function in between the Fibonacci instants \mathcal{N}^* and $\mathcal{N}^* + 1$ is generated by the sequence of kicks $S_{\mathcal{N}^*-1}$. Let us now denote the Fibonacci instants nested within the sequence $S_{\mathcal{N}^*-1}$ as \mathcal{M} , where $\mathcal{M} = 0, 1, 2, \dots, \mathcal{N}^* - 1$. The wave function of the rotor at these instants thus satisfies $|\psi_{N^*+F(\mathcal{M})}\rangle \approx U_{\text{Fi}}^{F(\mathcal{M})} |\psi_{N^*}\rangle$. Hence it straightaway follows that the wave function also remains localized at the instants $N^* + F(\mathcal{M})$, as the evolution is driven by the same effective Fibonacci Hamiltonian U_{Fi} . Proceeding similarly, one can argue that the sequence of kicks acting between $N = N^* + F(\mathcal{M}^*)$ and $N^* + F(\mathcal{M}^* + 1)$ is precisely the sequence $S_{\mathcal{M}^*-1}$ and hence the wave function

remains localized at the Fibonacci instants nested between $N = N^* + F(\mathcal{M}^*)$ and $N^* + F(\mathcal{M}^* + 1)$. Thus the quasilocalization is enforced in a self-similar way between two subsequent Fibonacci instants. In other words, the localized eigenstates of U_{Fi} act as *self-similar eigenstates* of $U(N, 0)$ and ultimately lead to the quasilocalized dynamics observed stroboscopically.

To further support the arguments presented above, we estimate the localization length $\langle \hat{l}^2 \rangle_{\text{loc}}$, with the initial state of the rotor being an angular momentum eigenstate, $|\psi_0\rangle = |l_0\rangle$, for simplicity in calculation. Assuming that $|\psi_{F(\mathcal{N})}\rangle \approx U_{\text{Fi}}^{F(\mathcal{N})} |l_0\rangle$ and $U_{\text{Fi}} = VDV^\dagger$, where D is a diagonal matrix, it can be shown that (see Appendix A)

$$\langle \hat{l}^2 \rangle_{\text{loc}} = \sum_{l,m} l^2 |V_{l0m}|^2 |V_{lm}|^2. \quad (8)$$

The localization length calculated using the above equation indeed turns out to be similar to that obtained from exact numerics. This is illustrated in the inset of Fig. 1(a), where the fluctuations in the kinetic energy for $N < 10^4$ are found to be evenly distributed about the mean value calculated using Eq. (8).

It is important to realize that higher-order terms in the BCH expansion, which we have ignored so far, can become significant under two conditions: (i) if the drive frequency is lowered, so that terms of order $O(\tau^2)$ become significant, and (ii) if the NECs of the higher-order commutator terms grow boundlessly so that such terms, although initially insignificant, start to dominate after a certain time has elapsed. As we shall see below, the second condition is particularly important as it explains both the ergodic behavior observed at low frequencies and the breakdown of the localization after sufficiently long time at high frequencies.

B. Emergence of diffusive behavior at low frequencies

Let us recall that the saturation of the NECs to steady values for $\mathcal{N} \gg 1$ is crucial for the existence of an effective Fibonacci Hamiltonian. Without explicitly determining all the commutator terms that may contribute when terms of order $\sim O(\tau^2)$ are included, let us analyze the expansion coefficients of the commutators $[L_1, [L_1, [L_1, L_2]]]$, $[L_2, [L_2, [L_1, L_2]]]$, and $[L_1, [L_2, [L_1, L_2]]]$. We denote the corresponding expansion coefficients as $\mu_1(N)$, $\mu_2(N)$, and $\mu_3(N)$, respectively. These NECs at $N = F(\mathcal{N})$ with $\mathcal{N} \gg 1$ are found to be [34]

$$\frac{\mu_1(F(\mathcal{N}))}{F(\mathcal{N})} = \frac{(-1)^{\mathcal{N}}}{120} \left[G^{\mathcal{N}-1} + \frac{1}{G} [(-1)^{\mathcal{N}}(3G-4) - 1 - 3G] \right], \quad (9a)$$

$$\frac{\mu_2(F(\mathcal{N}))}{F(\mathcal{N})} = \frac{(-1)^{\mathcal{N}}}{120} \left[G^{\mathcal{N}-1}(2-G) + \frac{1}{G} [(-1)^{\mathcal{N}}(4G-7) - 2 - G] \right], \quad (9b)$$

$$\frac{\mu_3(F(\mathcal{N}))}{F(\mathcal{N})} = \frac{(-1)^{\mathcal{N}}}{120} \left[2G^{\mathcal{N}-1}(1-G) + \frac{1}{G} [(-1)^{\mathcal{N}}(3-G) + 3 + 4G] \right], \quad (9c)$$

where we have ignored terms of order $G^{-(\mathcal{N}+1)}$, $G^{-(2\mathcal{N}+1)}$, $G^{-(3\mathcal{N}+1)}$, etc. It is immediately clear that the NECs defined above do not saturate to steady values even in the asymptotic

limit; rather, their growth with \mathcal{N} is unbounded. Indeed, it can be shown that this is true for all the NECs of higher-order nested commutators [34]. Thus we conclude that when the

frequency of the drive is low enough such that the contribution of higher-order terms become significant, the dynamics at Fibonacci instants is no longer governed by an effective Fibonacci Hamiltonian. The evolution of the rotor then mimics that of random driving, thereby leading to the emergence of ergodic behavior after sufficiently long times.

C. Crossover from the preergodic regime to the ergodic regime at high frequencies

The unbounded growth of the NECs in Eqs. (9a)–(9c) has a more important consequence. For $\tau \ll 1$, the higher-order terms containing the commutators corresponding to these NECs are insignificant when \mathcal{N} is not too large. However, it is easy to see that there will exist a long but finite time after which such terms will become significant and, consequently, the ergodic behavior will set in. This leads to the breakdown of the localization observed in the limit of high frequency. Indeed, one can perform an order-of-magnitude estimation of the time N_{deloc} , after which the diffusive growth is expected to manifest as follows. From Eqs. (9a)–(9c), we note that the leading-order term unbounded in \mathcal{N} grows as $G^{\mathcal{N}}/120$. The $O(\tau^2)$ terms in the expansion of Eq. (7) thus become significant when $\tau^2 G^{\mathcal{N}_{\text{deloc}}}/120 \sim 1$. For $\tau \approx 0.01$, this translates to $\mathcal{N}_{\text{deloc}} \approx 29$ or $N_{\text{deloc}} \approx 1.3 \times 10^6$. Thus, within the experimentally realizable time scale, one should observe the quasilocalization. This agrees remarkably well with the results found from exact numerical calculations [see Fig. 1(b)].

Finally, we note that the delocalization time $\mathcal{N}_{\text{deloc}}$ can be interpreted as the time required by the system to “resolve the randomness” of the quasiperiodic drive. The existence of the time-independent effective Hamiltonian for small τ , combined with the self-similarity of the drive, leads to an effective periodic evolution from the system’s point of view. Only at later times, when higher-order terms start to dominate and the effective time-independent Hamiltonian picture breaks down, does the system realize that the drive is not periodic and does diffusive dynamics set in.

V. SUMMARY

In conclusion, we have demonstrated that a quantum rotor driven with a binary Fibonacci sequence can exhibit both

diffusive and quasilocalized behavior. The latter manifests in the limit of high frequency of the drive, although diffusive behavior eventually sets in after sufficiently long times. It is interesting to note that the preergodic regime, within which the quasilocalization persists at high frequencies, is reminiscent of the *prethermal* regimes observed in out-of-equilibrium many-body quantum systems. In such systems, the presence of approximately conserved quantities prevents the system from thermalizing for a long period of time. An important question that arises is whether the dynamics of the FQKR can be mapped to a real-space lattice model describing spatial localization, just as the dynamics of the regular QKR is mappable to the one-dimensional Anderson problem. If a mapping does exist, it would be interesting to see how the quasilocalization observed in the FQKR manifests in the dual model. This is, however, beyond the scope of this paper.

ACKNOWLEDGMENTS

We acknowledge Markus Heyl for discussions and for very useful comments and suggestions. We acknowledge Utso Bhattacharya, Somnath Maity, and Anatoli Polkovnikov for useful discussions and comments. S. Bhattacharjee acknowledges CSIR, India, for financial support. S. Bandyopadhyay acknowledges financial support from PMRF, MHRD, India. A.D. acknowledges financial support from the SPARC program, MHRD, India, and SERB, DST, New Delhi, India.

APPENDIX A: REGULAR QUANTUM KICKED ROTOR

The regular QKR is represented by the Hamiltonian

$$H(t) = \frac{\hat{l}^2}{2I} + \mathcal{K} \cos \hat{\theta} \sum_{N=0}^{\infty} \delta(t - NT). \quad (\text{A1})$$

As discussed in Sec. II, the above Hamiltonian always exhibits dynamical localization, irrespective of the drive frequency [see Fig. 4(a)]. The Floquet propagator governing the evolution of the rotor at stroboscopic instants is given by

$$U_F = e^{-i\frac{\hat{l}^2}{2}\tau} e^{-i\mathcal{K}\cos\hat{\theta}}, \quad (\text{A2})$$

where $\tau = T/I$ is a dimensionless parameter and we have set $\hbar = 1$. Let us consider the eigenspectrum of the Floquet

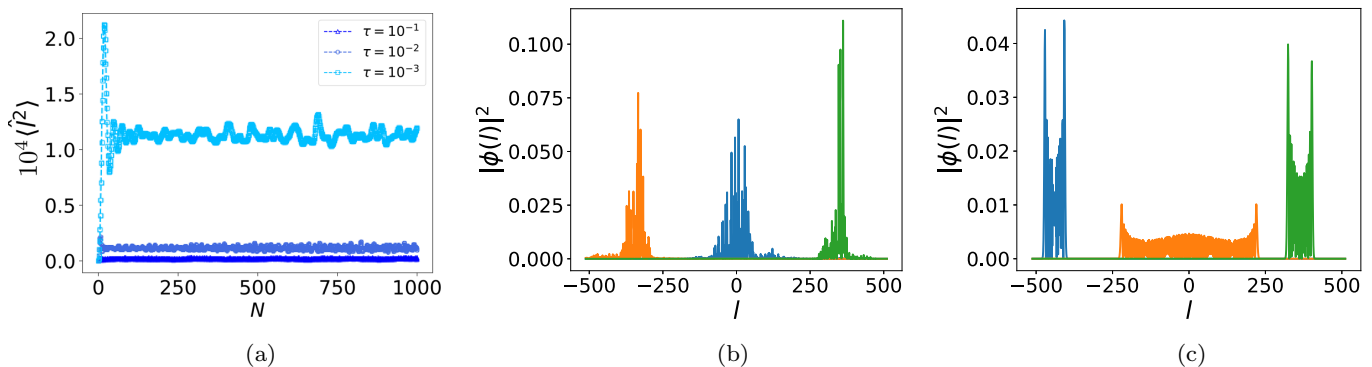


FIG. 4. (a) Evolution of the kinetic energy observed at stroboscopic instants N for a regular rotor, $\mathcal{K}_2 = 15$. The energy dynamically localizes for all driving frequencies, barring resonance conditions, which are not considered in this paper. (b) and (c) Typical eigenstates of the Floquet propagator U_F localized around different values of l , defined in Eq. (A2), with $\mathcal{K} = 15$ and kick frequency $\tau = 1$ (b) and $\tau = 0.001$ (c).

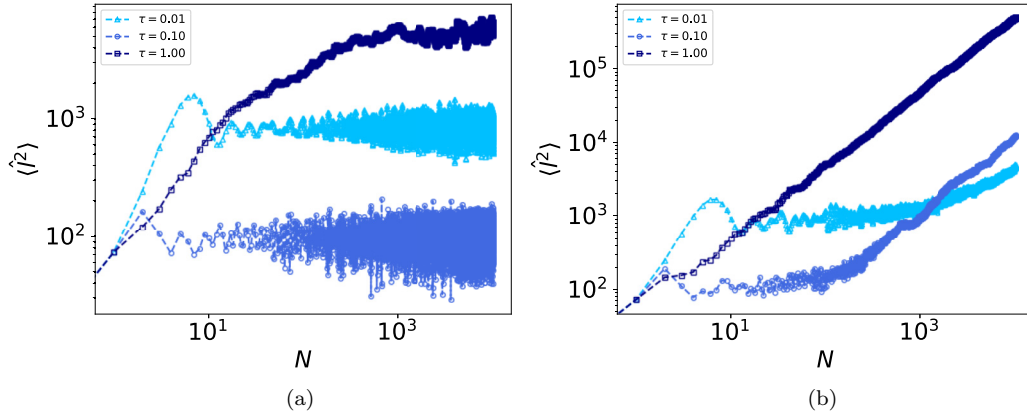


FIG. 5. (a) Evolution of the kinetic energy observed at stroboscopic instants N when the rotor is driven with (a) biperiodic and (b) aperiodic binary sequences and the kick amplitudes are chosen as $\mathcal{K}_1 = 10$ and $\mathcal{K}_2 = 12$. The energy saturates for all driving frequencies in the case of the biperiodic sequence, while it grows diffusively in the other case.

propagator: $U_F = \sum_m e^{i\phi_m} |\phi_m\rangle \langle \phi_m|$. As the Hilbert space dimension is infinite and the *quasienergies* ϕ_m are defined modulo 2π , the Floquet propagator has a dense eigenspectrum with ill-defined mean level spacing. However, as shown in Fig. 4(b), all the eigenstates $|\phi_m\rangle$ turn out to be exponentially localized in the angular momentum space, unless $\tau \ll 1$, which we shall consider shortly. To see how these properties lead to a dynamical localization in the dynamics, let us explicitly calculate the kinetic energy in terms of the matrix elements of the Floquet propagator. Without loss of generality, we assume that the rotor is initialized in a definite angular momentum state $|l_0\rangle$. The kinetic energy after N stroboscopic instants can then be evaluated as

$$\langle \hat{l}^2 \rangle = \langle l_0 | U_F^{N\dagger} \hat{l}^2 U_F^N | l_0 \rangle = \sum_{l,m,m'} l^2 e^{iN(\phi_m - \phi_{m'})} V_{l_0 m} V_{l m'}^* V_{l m} V_{l_0 m}^*,$$

where $V_{l_0 m} = \langle l_0 | \phi_m \rangle$ and so on. As the eigenstates are exponentially localized in the angular momentum basis, we have $V_{l l'} \approx 0$ for $|l - l'| > l_s$, where l_s is the *localization length* and is a measure of the number of Floquet eigenstates which overlaps with each angular momentum state. It is thus clear that in the equation above, only a finite number of eigenstates can contribute to the sum, resulting in the effective quasienergy spectrum being discrete with a mean level spacing of $2\pi/l_s$.

The onset of dynamical localization can now be explained as follows. If $2\pi N/l_s \gg 1$, all the oscillating terms in Eq. (A3) vanish; the average kinetic energy evaluates to

$$\langle \hat{l}^2 \rangle = \sum_{l,m} l^2 |V_{l_0 m}|^2 |V_{l m}|^2 \sim l_s^2 + l_0^2, \quad (\text{A3})$$

which is independent of N . Furthermore, the Heisenberg time, defined as the initial time for which the kinetic energy grows diffusively, can also be roughly approximated from $2\pi N^*/l_s \approx 1$ or $N^* \sim l_s$. As the kinetic energy is known to follow the classical dynamics till N^* with a diffusion constant $\sim \mathcal{K}_{cl}^2 = \mathcal{K}^2 \tau^2$, we have

$$\langle \hat{l}^2 \rangle \sim \mathcal{K}^2 \tau^2 N^* + l_0^2 \quad (\text{A4})$$

or

$$l_s^2 \sim \mathcal{K}^2 \tau^2 l_s, \quad (\text{A5})$$

which determines both the localization length and the Heisenberg time as

$$l_s \sim \mathcal{K}^2 \tau^2. \quad (\text{A6})$$

APPENDIX B: DYNAMICS OF THE ROTOR UNDER BIPERIODIC AND APERIODIC BINARY SEQUENCES

The dynamical quasilocalization observed in the case of the FQKR at high-frequency drives is not guaranteed for arbitrary binary sequences. To illustrate this, we consider a QKR driven with a biperiodic sequence with $K_N = \mathcal{K}_1(\mathcal{K}_2)$ for even (odd) N and an aperiodic binary sequence where the amplitude of the kick can either be \mathcal{K}_1 or \mathcal{K}_2 with equal probability at every stroboscopic instant. This is illustrated in Fig. 5, which shows that energy saturates for all driving frequencies in the case of the biperiodic sequence [see Fig. 5(a)] while it evolves diffusively in the case of the aperiodic sequence, $\langle \hat{l}^2 \rangle \propto N$, irrespective of the driving frequency [see Fig. 5(b)].

APPENDIX C: QUASILOCALIZATION DYNAMICS FOR DIFFERENT l_0

As discussed in Sec. III, the initial state of the rotor is chosen to be a coherent Gaussian state centered around the angular momentum l_0 , i.e., $\psi_0(l) = (\frac{2}{\pi})^{1/4} e^{-(l-l_0)^2}$. The numerical results presented in this paper correspond to $l_0 = 0$. To verify that the quasilocalization behavior observed is insensitive to the choice of l_0 , we plot the evolution of the kinetic energy for different values of l_0 in Fig. 6. We find that the choice of l_0 only alters the mean value of the kinetic energy in the preergodic phase.

APPENDIX D: HIGH-FREQUENCY EXPANSION OF THE UNITARY OPERATOR

In this Appendix, we shall derive the high-frequency expansion of the time-evolution unitary operator for a QKR when driven with a binary sequence of kicks. As discussed in Eq. (3) of Sec. II, the unitary operator driving the evolution

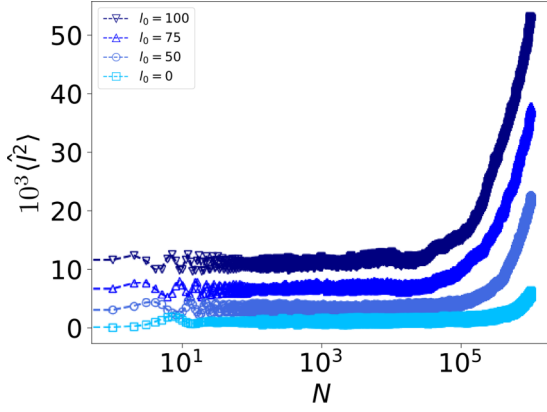


FIG. 6. Evolution of the kinetic energy for the FQKR with different choices of l_0 . The kick amplitudes are chosen to be $\mathcal{K}_1 = 10$ and $\mathcal{K}_2 = 12$.

between the $(N - 1)$ th and N th kicks is given by

$$U_n = e^{-i\frac{\tau}{2}} e^{-iK_N \cos \hat{\theta}}. \quad (\text{D1})$$

We recall that given a pair of noncommuting operators A and B , one can write $e^A e^B = e^C$, where C is given by the Baker-Campbell-Hausdorff formula,

$$C = A + B + \frac{1}{2}[A, B] + \frac{1}{12}([A, [A, B]] + [B, [B, A]]) + \dots \quad (\text{D2})$$

Substituting $A = -i\hat{p}^2\tau/2$ and $B = -iK_N \cos \hat{\theta}$, it is straightforward to check that the only commutators in the above expression which contribute up to linear order in τ are

$$[A, B] = -\frac{iK_N\tau}{2}(\hat{l} \sin \hat{\theta} + \sin \hat{\theta} \hat{l}) + O(\tau^2), \quad (\text{D3a})$$

$$[B, [B, A]] = -\frac{iK_N^2\tau}{2} \sin^2 \hat{\theta} + O(\tau^2). \quad (\text{D3b})$$

At high frequencies or $\tau \ll 1$, we can therefore neglect all other commutators in Eq. (D2). Recalling $K_N \in \{\mathcal{K}_1, \mathcal{K}_2\}$ for a binary sequence, we obtain

$$U_N \approx e^{-iL_{1,2}}, \quad (\text{D4a})$$

$$L_{1,2} = \mathcal{K}_{1,2} \cos \hat{\theta} + \frac{\tau}{2} \left[\hat{p}^2 + \frac{\mathcal{K}_{1,2}}{2} (\hat{l} \sin \hat{\theta} + \sin \hat{\theta} \hat{l}) + \frac{\mathcal{K}_{1,2}^2}{6} \sin^2 \hat{\theta} \right] + O(\tau^2). \quad (\text{D4b})$$

Let us now consider the evolution of the QKR when driven with a Fibonacci sequence of kicks. For $\tau \ll 1$ such that Eqs. (D4a) and (D4b) are satisfied, the evolution operator assumes the form

$$U(N, 0) = \dots e^{-iL_2} e^{-iL_1} e^{-iL_2} e^{-iL_1} e^{-iL_2} e^{-iL_1}. \quad (\text{D5})$$

Our purpose is to derive an approximate expression for the evolution operator by progressively approximating the unitary operator for adjacent time intervals. Let us denote the evolution over the first two time intervals: $U(2, 0) \approx e^{-iL_2} e^{-iL_1} =$

$e^{-i\Theta_{12}}$, where Θ_{12} is to be computed using the BCH formula. As before, we calculate the commutators

$$[-iL_2, -iL_1] = i(\mathcal{K}_2 - \mathcal{K}_1) \frac{\tau}{2} (\hat{l} \sin \hat{\theta} + \sin \hat{\theta} \hat{l}) + O(\tau^2), \quad (\text{D6a})$$

$$[-iL_1, [-iL_1, -iL_2]] = i\mathcal{K}_1(\mathcal{K}_2 - \mathcal{K}_1)\tau \sin^2 \hat{\theta} + O(\tau^2), \quad (\text{D6b})$$

$$[-iL_2, [-iL_2, -iL_1]] = -i\mathcal{K}_2(\mathcal{K}_2 - \mathcal{K}_1)\tau \sin^2 \hat{\theta} + O(\tau^2). \quad (\text{D6c})$$

It can be straightforwardly verified from the above expressions that all other higher-order commutators, such as $[L_1, [L_1, [L_1, L_2]]]$, will contribute terms which are at least quadratic in order τ . Retaining terms up to linear order in τ , we find

$$-i\Theta_{12} = -i\beta(2)L_2 - i\alpha(2)L_1 + \delta(2)[-iL_2, -iL_1] \times \eta_1(2)[-iL_1, [-iL_1, -iL_2]] + \eta_2(2)[-iL_2, [-iL_2, -iL_1]],$$

where $\alpha(2) = \beta(2) = 1$, $\delta(2) = 1/2$, and $\eta_1(2) = \eta_2(2) = 1/12$.

We can now build the unitary operator as follows. After three kicks, the evolution operator can be approximated as $U(3, 0) = e^{-iL_1} e^{-i\Theta_{12}} = e^{-i\Theta_{13}}$, where Θ_{13} is found to be

$$-i\Theta_{13} = -2iL_1 - iL_2 - \frac{1}{6}[-iL_1, [-iL_1, -iL_2]] + \frac{1}{6}[-iL_2, [-iL_2, -iL_1]]. \quad (\text{D7})$$

A careful inspection reveals that when the N th kick is \mathcal{K}_1 , the expansion coefficients obey the following recursion relations:

$$\delta(N) = \delta(N-1) - \frac{1}{2}\beta(N-1), \quad (\text{D8a})$$

$$\eta_1(N) = \eta_1(N-1) - \frac{1}{2}\delta(N-1) + \frac{1}{12}\beta(N-1)(1 - \alpha(N-1)), \quad (\text{D8b})$$

$$\eta_2(N) = \eta_2(N-1) + \frac{1}{12}\beta^2(N-1). \quad (\text{D8c})$$

Conversely, when the N th kick is \mathcal{K}_2 , the recursion relations are given by

$$\delta(N) = \delta(N-1) + \frac{1}{2}\alpha(N-1), \quad (\text{D9a})$$

$$\eta_1(N) = \eta_1(N-1) + \frac{1}{12}\alpha^2(N-1), \quad (\text{D9b})$$

$$\eta_2(N) = \eta_2(N-1) + \frac{1}{2}\delta(N-1) + \frac{1}{12}\alpha(N-1)(1 - \beta(N-1)). \quad (\text{D9c})$$

To verify the above recursion relations, we explicitly calculate Θ_{14} and Θ_{15} as in Eq. (D7),

$$-i\Theta_{14} = -3iL_1 - iL_2 - \frac{1}{2}[-iL_2, -iL_1]$$

$$\begin{aligned}
& -\frac{1}{4}[-iL_1, [-iL_1, -iL_2]] \\
& +\frac{1}{4}[-iL_2, [-iL_2, -iL_1]], \quad (D10)
\end{aligned}$$

$$\begin{aligned}
-i\Theta_{15} &= -3iL_1 - 2iL_2 + [-iL_2, -iL_1] \\
& +\frac{1}{2}[-iL_1, [-iL_1, -iL_2]]. \quad (D11)
\end{aligned}$$

We recall from Eq. (D5) that the fourth and fifth kicks in the Fibonacci sequence are \mathcal{K}_1 and \mathcal{K}_2 , respectively. Thus the expansion coefficients in Θ_{14} and Θ_{15} satisfy the recursion relations given in Eqs. (D8a)–(D8c) and (D9a)–(D9c), respectively.

The recursion relations in Eqs. (D8a)–(D8c) and (D9a)–(D9c) can be unified using the generating function of the binary Fibonacci sequence, defined as

$$\gamma(N) = \lfloor (N+1)G \rfloor - \lfloor NG \rfloor, \quad (D12)$$

where $G = (\sqrt{5} + 1)/2$ is the golden ratio and $\lfloor x \rfloor$ denotes the greatest integer less than or equal to x . For any positive integer N , $\gamma(N) \in \{1, 2\}$. The function $\gamma(N) - 1$ is therefore a Boolean function, and it generates the required Fibonacci sequence. We show this below by explicitly evaluating it for $N = 1, 2, 3, \dots, 13$: Substituting \mathcal{K}_1 and \mathcal{K}_2 in place of 1 and 0 in the second row of the table above, we recover the Fibonacci sequence defined in Eq. (5) of Sec. II.

N	1	2	3	4	5	6	7	8	9	10	11	12	13
$\gamma(N) - 1$	1	0	1	1	0	1	0	1	1	0	1	1	0

Using the generating function $\gamma(N)$ defined above, the coefficients $\beta(N)$ and $\alpha(N)$ are immediately evaluated as

$$\beta(N) = \sum_{n=1}^N (2 - \gamma(n)), \quad (D13a)$$

$$\alpha(N) = \sum_{n=1}^N (\gamma(n) - 1) = N - \beta(N). \quad (D13b)$$

Having evaluated $\alpha(N)$ and $\beta(N)$, the recursion relation for $\delta(N)$ can be simplified to

$$\delta(N) = \sum_{n=1}^N \left[(2 - \gamma(n)) \frac{\alpha(n-1)}{2} - (\gamma(n) - 1) \frac{\beta(n-1)}{2} \right], \quad (D14)$$

where $\alpha(0) = \beta(0) = 0$. Furthermore, it can be verified that if $\gamma(n) = 2$, then $\beta(n-1) = \lfloor n/(1+G) \rfloor$. Similarly, if $\gamma(n) = 1$, then $\alpha(n-1) = \lfloor nG/(1+G) \rfloor$. Substituting in the above expression, we therefore find

$$\delta(N) = -\frac{1}{2} \sum_{n=1}^N \left[(\gamma(n) - 1)(n-1) - \left\lfloor \frac{nG}{1+G} \right\rfloor \right], \quad (D15)$$

where we have used the relation $\lfloor nG/(1+G) \rfloor + \lfloor n/(1+G) \rfloor = n-1$. Finally, the coefficients $\eta_1(N)$ and $\eta_2(N)$ can be evaluated as

$$\eta_1(N) = \frac{1}{12} \sum_{m=1}^N \left[(2 - \gamma(m)) \left\lfloor \frac{nG}{1+G} \right\rfloor^2 (1 - \gamma(m)) \left(6\delta(m-1) - (2-m) \left\lfloor \frac{n}{1+G} \right\rfloor - \left\lfloor \frac{n}{1+G} \right\rfloor^2 \right) \right],$$

$$\eta_2(N) = \frac{1}{12} \sum_{m=1}^N \left[(\gamma(m) - 1) \left\lfloor \frac{n}{1+G} \right\rfloor^2 (2 - \gamma(m)) \left(6\delta(m-1) + (2-m) \left\lfloor \frac{nG}{1+G} \right\rfloor + \left\lfloor \frac{nG}{1+G} \right\rfloor^2 \right) \right].$$

APPENDIX E: EMERGENCE OF EFFECTIVE FIBONACCI HAMILTONIAN

As discussed in Sec. IV, the NECs for terms up to order $O(\tau)$ either saturate to steady values or oscillate when observed at Fibonacci instants. Indeed, using the so-called ‘‘local deflation rule’’ for the Fibonacci sequence, one can show that the asymptotic values of the NECs for $\mathcal{N} \gg 1$ are given by [34]

$$\frac{\alpha(F(\mathcal{N}))}{F(\mathcal{N})} = \frac{1}{G}, \quad (E1a)$$

$$\frac{\beta(F(\mathcal{N}))}{F(\mathcal{N})} = \frac{1}{G^2}, \quad (E1b)$$

$$\frac{\delta(F(\mathcal{N}))}{F(\mathcal{N})} = -\frac{1}{G^3}, \quad (E1c)$$

$$\frac{\eta_1(F(\mathcal{N}))}{F(\mathcal{N})} = \frac{1}{12} \left[\frac{1}{G^4} + (-1)^{\mathcal{N}} \left(\frac{2}{G} + \frac{1}{G^2} \right) \right], \quad (E1d)$$

$$\frac{\eta_2(F(\mathcal{N}))}{F(\mathcal{N})} = \frac{1}{12} \left[\frac{1}{G^5} - (-1)^{\mathcal{N}} \left(\frac{2}{G^2} + \frac{1}{G^3} \right) + \frac{1}{G^2} \right]. \quad (E1e)$$

We shall henceforth denote the saturation values of the NECs at Fibonacci instants as $\bar{\alpha}$, $\bar{\beta}$, $\bar{\delta}$, $\bar{\eta}_1$, $\bar{\eta}_2$, where $\bar{\eta}_1$ and $\bar{\eta}_2$ correspond to the mean of the oscillating values of $\eta_1(N)/N$ and $\eta_2(N)/N$, respectively. Substituting the saturation values derived above, the propagator at Fibonacci instants $U_{F(\mathcal{N})}$ can be expressed in terms of an *effective Fibonacci propagator* U_{Fi} , such that

$$U_{N=F(\mathcal{N})} \approx U_{\text{Fi}}^{F(\mathcal{N})} = e^{-iH_{\text{Fi}}F(\mathcal{N})}, \quad (E2a)$$

where

$$\begin{aligned}
H_{\text{Fi}} &= \bar{\alpha}L_1 + \bar{\beta}L_2 + \bar{\delta}[L_2, L_1] \\
& + \bar{\eta}_1[L_1, [L_1, L_2]] + \bar{\eta}_2[L_2, [L_2, L_1]] \quad (E2b)
\end{aligned}$$

is defined as the *effective Fibonacci Hamiltonian*.

- [1] B. V. Chirikov, A universal instability of many-dimensional oscillator systems, *Phys. Rep.* **52**, 263 (1979).
- [2] F. M. Izrailev, Simple models of quantum chaos: Spectrum and eigenfunctions, *Phys. Rep.* **196**, 299 (1990).
- [3] G. Casati, B. V. Chirikov, F. M. Izrailev, and J. Ford, Stochastic behavior of a quantum pendulum under a periodic perturbation, in *Stochastic Behavior in Classical and Quantum Hamiltonian Systems*, edited by G. Casati and J. Ford (Springer, Berlin, 1979), p. 334.
- [4] S. Fishman, D. R. Grempel, and R. E. Prange, Chaos, Quantum Recurrences, and Anderson Localization, *Phys. Rev. Lett.* **49**, 509 (1982).
- [5] D. R. Grempel, R. E. Prange, and S. Fishman, Quantum dynamics of a nonintegrable system, *Phys. Rev. A* **29**, 1639 (1984).
- [6] S.-J. Chang and K.-J. Shi, Evolution and exact eigenstates of a resonant quantum system, *Phys. Rev. A* **34**, 7 (1986).
- [7] S. Fishman, D. R. Grempel, and R. E. Prange, Temporal crossover from classical to quantum behavior near dynamical critical points, *Phys. Rev. A* **36**, 289 (1987).
- [8] S. Fishman, R. E. Prange, and M. Griniasty, Scaling theory for the localization length of the kicked rotor, *Phys. Rev. A* **39**, 1628 (1989).
- [9] E. J. Galvez, B. E. Sauer, L. Moorman, P. M. Koch, and D. Richards, Microwave Ionization of H Atoms: Breakdown of Classical Dynamics for High Frequencies, *Phys. Rev. Lett.* **61**, 2011 (1988).
- [10] J. E. Bayfield, G. Casati, I. Guarneri, and D. W. Sokol, Localization of classically chaotic diffusion for hydrogen atoms in microwave fields, *Phys. Rev. Lett.* **63**, 364 (1989).
- [11] F. L. Moore, J. C. Robinson, C. Bharucha, P. E. Williams, and M. G. Raizen, Observation of Dynamical Localization in Atomic Momentum Transfer: A New Testing Ground for Quantum Chaos, *Phys. Rev. Lett.* **73**, 2974 (1994).
- [12] F. L. Moore, J. C. Robinson, C. F. Bharucha, B. Sundaram, and M. G. Raizen, Atom Optics Realization of the Quantum δ -Kicked Rotor, *Phys. Rev. Lett.* **75**, 4598 (1995).
- [13] H. Ammann, R. Gray, I. Shvachuck, and N. Christensen, Quantum Delta-Kicked Rotor: Experimental Observation of Decoherence, *Phys. Rev. Lett.* **80**, 4111 (1998).
- [14] M. Bitter and V. Milner, Experimental Observation of Dynamical Localization in Laser-Kicked Molecular Rotors, *Phys. Rev. Lett.* **117**, 144104 (2016).
- [15] S. Sarkar, S. Paul, C. Vishwakarma, S. Kumar, G. Verma, M. Sainath, U. D. Rapol, and M. S. Santhanam, Nonexponential Decoherence and Subdiffusion in Atom-Optics Kicked Rotor, *Phys. Rev. Lett.* **118**, 174101 (2017).
- [16] H.-J. Stockmann, *Quantum Chaos: An Introduction* (Cambridge University Press, Cambridge, 1999).
- [17] F. Haake, S. Gnutzmann, and M. Kuś, *Quantum Signatures of Chaos*, 4th ed. (Springer, Cham, Switzerland, 2018).
- [18] L. D'Alessio, Y. Kafri, A. Polkovnikov, and M. Rigol, From quantum chaos and eigenstate thermalization to statistical mechanics and thermodynamics, *Adv. Phys.* **65**, 239 (2016).
- [19] M. S. Santhanam, S. Paul, and J. B. Kannan, Quantum kicked rotor and its variants: Chaos, localization and beyond, *Phys. Rep.* **956**, 1 (2022).
- [20] G. Floquet, Sur les equations differentielles lineaires a coefficients periodiques, *Ann. Sci. École Norm. Super.* **12**, 47 (1883).
- [21] J. H. Shirley, Solution of the Schrödinger Equation with a Hamiltonian Periodic in Time, *Phys. Rev.* **138**, B979 (1965).
- [22] M. Bukov, L. D'Alessio, and A. Polkovnikov, Universal high-frequency behavior of periodically driven systems: from dynamical stabilization to Floquet engineering, *Adv. Phys.* **64**, 139 (2015).
- [23] A. Eckardt, Colloquium: Atomic quantum gases in periodically driven optical lattices, *Rev. Mod. Phys.* **89**, 011004 (2017).
- [24] P. W. Anderson, Absence of Diffusion in Certain Random Lattices, *Phys. Rev.* **109**, 1492 (1958).
- [25] E. Abrahams, P. W. Anderson, D. C. Licciardello, and T. V. Ramakrishnan, Scaling Theory of Localization: Absence of Quantum Diffusion in Two Dimensions, *Phys. Rev. Lett.* **42**, 673 (1979).
- [26] The kinetic energy terms in the Hamiltonian of the three-dimensional rotor are linear in momentum in two of the orthogonal directions.
- [27] G. Casati, I. Guarneri, and D. L. Shepelyansky, Anderson Transition in a One-Dimensional System with Three Incommensurate Frequencies, *Phys. Rev. Lett.* **62**, 345 (1989).
- [28] H. M. Morse, Recurrent geodesics on a surface of negative curvature, *Trans. Am. Math. Soc.* **22**, 84 (1921).
- [29] H. M. Morse, A one-to-one representation of geodesics on a surface of negative curvature, *Am. J. Math.* **43**, 33 (1921).
- [30] M. Kohmoto, L. P. Kadanoff, and C. Tang, Localization Problem in One Dimension: Mapping and Escape, *Phys. Rev. Lett.* **50**, 1870 (1983).
- [31] S. Ostlund, R. Pandit, D. Rand, H. J. Schellnhuber, and E. D. Siggia, One-Dimensional Schrödinger Equation with an Almost Periodic Potential, *Phys. Rev. Lett.* **50**, 1873 (1983).
- [32] B. Sutherland, Simple System with Quasiperiodic Dynamics: A Spin in a Magnetic Field, *Phys. Rev. Lett.* **57**, 770 (1986).
- [33] S. Nandy, A. Sen, and D. Sen, Aperiodically Driven Integrable Systems and Their Emergent Steady States, *Phys. Rev. X* **7**, 031034 (2017).
- [34] P. T. Dumitrescu, R. Vasseur, and A. C. Potter, Logarithmically Slow Relaxation in Quasiperiodically Driven Random Spin Chains, *Phys. Rev. Lett.* **120**, 070602 (2018).
- [35] S. Nandy, A. Sen, and D. Sen, Steady states of a quasiperiodically driven integrable system, *Phys. Rev. B* **98**, 245144 (2018).
- [36] S. Maity, U. Bhattacharya, A. Dutta, and D. Sen, Fibonacci steady states in a driven integrable quantum system, *Phys. Rev. B* **99**, 020306(R) (2019).
- [37] S. Ray, S. Sinha, and D. Sen, Dynamics of quasiperiodically driven spin systems, *Phys. Rev. E* **100**, 052129 (2019).
- [38] B. Mukherjee, A. Sen, D. Sen, and K. Sengupta, Restoring coherence via aperiodic drives in a many-body quantum system, *Phys. Rev. B* **102**, 014301 (2020).
- [39] P. Zhang and Y. Gu, Periodically and quasi-periodically driven dynamics of Bose-Einstein condensates, *SciPost Phys.* **9**, 079 (2020).
- [40] H. Zhao, F. Mintert, R. Moessner, and J. Knolle, Random Multipolar Driving: Tunably Slow Heating through Spectral Engineering, *Phys. Rev. Lett.* **126**, 040601 (2021).
- [41] J. Ringot, P. Szriftgiser, J. C. Garreau, and D. Delande, Experimental Evidence of Dynamical Localization and Delocalization in a Quasiperiodically Driven System, *Phys. Rev. Lett.* **85**, 2741 (2000).

[42] An alternate common way of representing the evolution operator is $U_N = \exp[-i\frac{\hat{p}^2}{2\hbar_s}] \exp[-i\frac{\tilde{K}_N}{\hbar_s} \cos \hat{\theta}]$, where $\hbar_s = \hbar T/I$ is the effective Planck's constant, $\hat{p} = \hbar_s \hat{l}$, and $\tilde{K}_N = K_N \hbar_s$. We

work with natural units $\hbar = 1$ and set $T/I = \tau$, which implies that τ can equivalently be considered as the effective Planck's constant.